Chemical Science

rsc.li/chemical-science



ISSN 2041-6539



Chemical Science



EDGE ARTICLE

View Article Online
View Journal | View Issue



Cite this: Chem. Sci., 2019, 10, 3161

d All publication charges for this article have been paid for by the Royal Society of Chemistry

Received 16th December 2018 Accepted 11th February 2019

DOI: 10.1039/c8sc05608k

rsc.li/chemical-science

Hydroxyl-mediated ethanol selectivity of CO₂ hydrogenation†

Chengsheng Yang,‡ Rentao Mu,‡ Guishuo Wang, Jimin Song, Hao Tian, Zhi-Jian Zhao and Jinlong Gong **

Oxide-supported Rh nanoparticles have been widely used for CO_2 hydrogenation, especially for ethanol synthesis. However, this reaction operates under high pressure, up to 8 MPa, and suffers from low CO_2 conversion and alcohol selectivity. This paper describes the crucial role of hydroxyl groups bound on Rh-based catalysts supported on TiO_2 nanorods (NRs). The RhFeLi/ TiO_2 NR catalyst shows superior reactivity (\approx 15% conversion) and ethanol selectivity (32%) for CO_2 hydrogenation. The promoting effect can be attributed to the synergism of high Rh dispersion and high-density hydroxyl groups on TiO_2 NRs. Hydroxyls are proven to stabilize formate species and protonate methanol, which is easily dissociated into *CH_x , and then CO obtained from the reverse water–gas shift reaction (RWGS) is inserted into *CH_x to form CH_3CO^* , followed by CH_3CO^* hydrogenation to ethanol.

Introduction

Carbon dioxide (CO_2) is one of the major components of greenhouse gases, which can result in climate change and ocean acidification. Among the different approaches explored for controlling CO_2 emission, the chemical conversion of CO_2 to high-value-added fuels (oxygenates, alcohols, olefins *etc.*) has attracted extensive attention.¹⁻⁴ Compared with C_1 products (CO, CH_4 and CH_3OH), the higher alcohols ($C_{2+}OH$, especially C_2H_5OH), which are mostly produced from biological fermentation, are widely applied in industries as indispensable higher-energy-density engine fuels and fuel additives.¹ According to thermodynamic analysis, the formation of ethanol from CO_2 is limited enormously at 1–30 bar due to the preferential production of CO or CH_4 , thus the selectivity to ethanol is relatively low.⁴

Therefore, the production of $C_{2+}OH$ by CO_2 hydrogenation is appealing but remains very challenging. Previous studies have shown that a Pt/Co_3O_4 catalyst⁵ achieved 27.3% selectivity to $C_{2+}OH$ with H_2O/DMI as a solvent. Multi-functional composite catalysts, such as $CoMoS^6$ (5.5% selectivity to ethanol), physically mixed Fe-based and Cu-based catalysts⁷ (17.4% selectivity to ethanol) and K/Cu-Zn-Fe catalysts^{8,9} (19.5% selectivity to $C_{2+}OH$ and CH_3OH), were also used for alcohol synthesis. Particularly, Rh-based catalysts have been evaluated as

Key Laboratory for Green Chemical Technology of Ministry of Education, School of Chemical Engineering and Technology, Tianjin University, Collaborative Innovation Center of Chemical Science and Engineering, Tianjin 300072, China. E-mail: jlgong@tju.edu.cn

promising catalysts for the selective synthesis of ethanol.^{4,10,11} In general, promoters such as Fe and Li are frequently used for enhancing ethanol selectivity *via* changing the electronic state of Rh and increasing the intensity of bridge-bonded CO species. For example, 5 wt% RhFe¹⁰ and RhLi¹¹ supported on SiO₂ showed ethanol selectivities of 16.4% and 15.5%, respectively.

However, there are still some limitations for alcohol production through CO2 hydrogenation reaction, such as the difficulties in CO2 activation, high energy barrier for C-O bond scission and the formation of C₁ by-products. Therefore, the design of efficient heterogeneous catalysts for ethanol production is of great importance. Tuning the particle size of noble metals can often increase the CO2 conversion and product selectivity.12-16 For example, suitable reducible metal oxide supports, such as TiO2 and ZrO2, have been extensively applied to tune the particle size. 17,18 The Au/TiO2 catalyst with abundant oxygen vacancies exhibited high selectivity to ethanol from CO2 reduction in DMF solvent.19 The bimetallic Pd2Cu/P25 catalyst also presented an excellent yield of ethanol with the help of water.20 On the other hand, a promotion strategy via hydroxyl groups has also been proved to be an efficient approach towards improving alcohol selectivity in CO hydrogenation.21-23

This work shows that a high yield of ethanol under low pressure can be achieved by the introduction of hydroxyls onto a TiO_2 support. First, 1 wt% RhFeLi (Rh: Fe: Li = 1:1:1) catalysts supported on a series of reducible oxides were prepared. The catalysts supported on TiO_2 nanorods (NRs) display the highest selectivity to ethanol. Since TiO_2 NRs have been extensively used in a variety of catalytic systems, such as photocatalytic water splitting, CO_2 photoreduction and dissociation of CO_2 to CO_2^{24-26} we synthesized TiO_2 NRs by a modified hydrothermal method. More importantly, high-density surface

 $[\]dagger$ Electronic supplementary information (ESI) available: Experimental details and supporting figures and tables. See DOI: 10.1039/c8sc05608k

[‡] These authors contributed equally to this work.

Chemical Science Edge Article

hydroxyls can be introduced into the catalytic system after reduction of ${\rm TiO_2}$ NR-supported catalysts in ${\rm H_2}$. A significant improvement of ethanol yield is observed for Rh-based catalysts supported on ${\rm TiO_2}$ NRs, which have not been reported in previous studies. Furthermore, the hydroxyl-mediated mechanism of ethanol formation over RhFeLi/TiO₂ NRs catalysts is investigated.

Results and discussion

Catalyst structure

The morphology of the synthesized TiO₂ NRs is shown in Fig. 1a and S1.† The length and diameter of TiO2 NRs are 50-200 nm and 10-20 nm, respectively. The specific surface area of TiO2 NRs is determined to be 23.6 $\text{m}^2\,\text{g}_{\text{cat}}^{-1}$, which is close to that of commercial ${\rm TiO_2}$ (${\rm TiO_2}$ Com, 18.2 m 2 ${\rm g_{cat}}^{-1}$) (Table S1†). The Rh-based catalysts supported on TiO2 NRs and TiO2 Com were prepared by incipient wetness impregnation. The Rh nanoparticles on TiO2 NRs present uniform size distribution with an average diameter of 2.3 \pm 1.0 nm (Fig. 1a, c and e). The highresolution images of Rh nanoparticles shown in Fig. 1c and d present a lattice distance of 0.23 nm, corresponding to Rh (111) planes.27 In contrast, two-times-larger (~4.0 nm) Rh nanoparticles in the range of 1-7 nm are observed on TiO2 Com (Fig. 1b, d and f). TEM studies indicate that TiO2 NRs can prevent the severe agglomeration of Rh nanoparticles after the reduction at 400 °C in a H2 atmosphere.

In XRD measurements, no characteristic peak of Fe₂O₃ can be found for RhFeLi/TiO₂ Com and RhFeLi/TiO₂ NRs when the

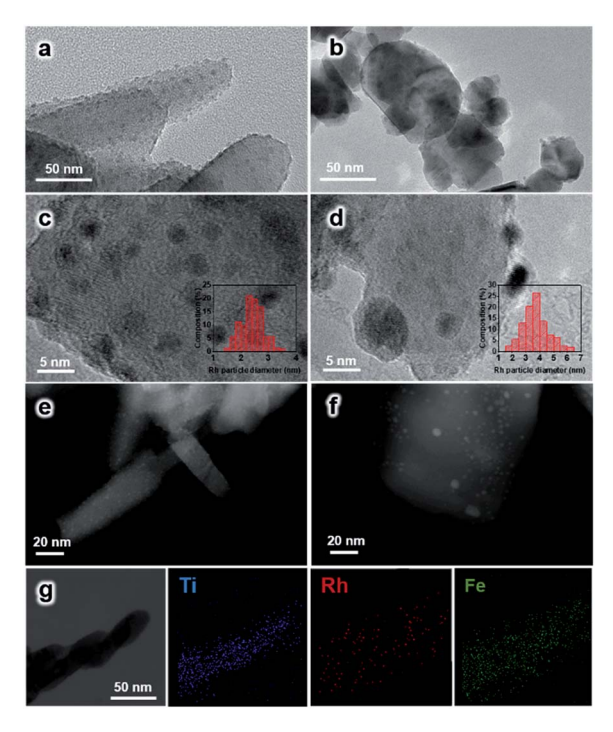


Fig. 1 (a and b) TEM; (c and d) HRTEM images, particle size distributions (inset figures) and (e and f) HAADF-STEM images of catalysts after reaction. (a, c and e) 2.5 wt% RhFeLi supported on $\rm TiO_2$ NRs and (b, d and f) 2.5 wt% RhFeLi supported on $\rm TiO_2$ Com. (g) STEM-EDS elemental mapping of 2.5 wt% RhFeLi supported on $\rm TiO_2$ NRs.

loading of Fe is relatively low (\sim 1 wt%) (Fig. 2). When the loading of Fe is increased to 2.5 wt%, the diffraction peak of Fe₂O₃ at 33.2° can be seen for TiO₂ Com. However, the diffraction peak of Fe₂O₃ does not appear for TiO₂ NRs even though the loading of Fe is increased to 5 wt% (Fig. 2). XRD results indicate that the dispersion of FeO_x over TiO₂ NRs is higher than that over TiO2 Com. EDS elemental mapping of RhFeLi/ TiO₂ NRs also shows that the FeO_r species are well dispersed on TiO₂ NRs (Fig. 1g). We note that no Raman shift of TiO₂ can be observed for all catalysts (Fig. S2†), indicating that the FeO_x species are deposited on the surface rather than being doped into TiO₂ bulk. The H₂ temperature-programmed reduction (H₂-TPR) results of FeO_x/TiO₂ show that the reduction temperature of FeO_x over TiO₂ NRs is 100 °C higher than the reduction temperature of FeO_x over TiO₂ Com (Fig. S3a†), suggesting that the FeO_x species are better dispersed on TiO₂ NRs compared with TiO2 Com.

 ${
m H_2}$ -TPR studies of RhFeLi/TiO $_2$ NRs and RhFeLi/TiO $_2$ Com were also carried out to investigate the interfacial interaction between Rh and oxide promoters (Fig. S3b†). According to previous studies, ¹⁰ the peaks below 200 °C can be ascribed to the reduction of Rh $_2$ O $_3$, while the broad peak appearing at higher temperature (300–500 °C) can be assigned to the reduction of Fe $_2$ O $_3$. We find that the reduction temperature of Rh $_2$ O $_3$ for RhFeLi/TiO $_2$ NRs is 50 °C higher than that on RhFeLi/TiO $_2$ Com, illustrating smaller Rh size on TiO $_2$ NRs. ¹⁴ As such, the higher dispersion of Rh-based nanoparticles on TiO $_2$ NRs should increase the number of interfacial sites between Rh and oxide promoters, where C–C coupling occurs *via* reaction between CO and *CH $_x$. ³⁻⁷

To further illustrate the surface structure of RhFeLi/TiO₂ NRs and RhFeLi/TiO₂ Com catalysts, CO titration experiments were

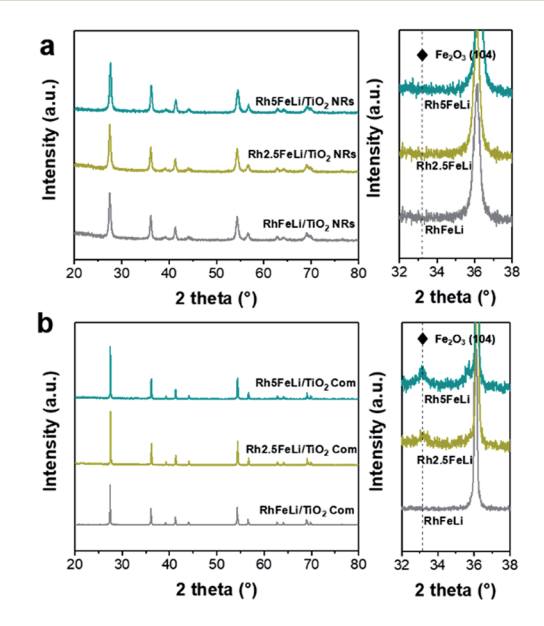


Fig. 2 (a) XRD spectra of 2.5 wt% RhFeLi/ TiO_2 NRs with different Fe loadings. (b) XRD spectra of 2.5 wt% RhFeLi/ TiO_2 Com with different Fe loadings. The figures on the right of (a) and (b) show the enlarged XRD patterns.

conducted. The active loop volume of CO for RhFeLi/TiO2 Com (0.09 cm³ g⁻¹), which is consumed by CO adsorption on Rh, is much smaller than that for RhFeLi/TiO₂ NRs (0.69 cm³ g⁻¹) (Table S2†). The observed low adsorption amount of CO on RhFeLi/TiO2 Com may be due to the partial encapsulation of Rh sites by oxide overlayers. The TEM image also shows that the Rh nanoparticles are decorated by oxide overlayers in the RhFeLi/TiO₂ Com catalyst (Fig. 1d). Quantitative XPS analysis was also conducted to investigate the surface structure of Rhbased catalysts (Table S3†). The surface molar ratio of Rh: Fe in RhFeLi/TiO2 NRs is determined to be 58: 42, which is close to the bulk molar ratio of Rh: Fe measured by ICP-AES (48:52) and the initial feed ratio. For RhFeLi/TiO2 Com, XPS investigations show that the surface molar ratio of Rh: Fe is 29:71. However, the bulk molar ratio of Rh: Fe determined by ICP-AES (Rh: Fe = 50:50) still agrees with the initial feed ratio, suggesting that the Rh nanoparticles should be partially covered by the FeO_x species. Note that the binding energy (BE) of Rh $3d_{5/2}$ locates at ~ 307.0 eV (Fig. S4b†), corresponding to the metallic state of Rh.28

Catalytic performance

Edge Article

The catalytic performance of Rh-based catalysts supported on different oxide supports in CO2 hydrogenation is studied. The TiO2 NR-supported catalysts present the highest ethanol yield (Fig. S5†). Additionally, a series of Rh-based catalysts with different promoters were synthesized. Compared with the mono-component Rh/TiO2 catalyst, the selectivity of RhFe/TiO2 for ethanol is improved significantly (16% for RhFe/TiO2 Com and 25% for RhFe/TiO₂ NRs, Fig. S6†). With an increase of the loading of Fe, CO2 conversion and the selectivity to ethanol and CH₄ decreased while the selectivity to CO increased (Fig. S7†). Since FeO_x could catalyze the reverse water-gas shift reaction (RWGS) to produce CO, the changes of CO₂ conversion and product distribution indicate that the excess Fe species has a passive effect on CO₂ conversion and ethanol synthesis by blocking the active Rh sites.10 This blocking effect may be caused by the encapsulation of Rh sites by FeOx species, which has been proven by XPS measurements combined with CO chemisorption (Table S2†). On the other hand, the addition of Li can increase the CO₂ conversion on Rh/TiO₂ by 5%, while the selectivity to ethanol does not change (Fig. S6c†). Based on these results, we conclude that the addition of Fe can promote the ethanol selectivity, while the addition of Li as an electronic promoter accelerates the CO₂ conversion. As such, higher ethanol selectivity and CO2 conversion are obtained by adding binary promoters *i.e.*, Fe and Li (Fig. S6d \dagger).

More interestingly, we show that the ethanol selectivity and CO_2 conversion over RhFeLi/TiO $_2$ NRs are much higher than those over RhFeLi/TiO $_2$ Com at 250 °C (Fig. S7†). For example, the 2.5 wt% RhFeLi/TiO $_2$ NR (Rh: Fe: Li = 1:1:1) catalyst presents more than 30% ethanol selectivity and 15% CO_2 conversion, which is about seven-fold higher ethanol yield than that on 2.5 wt% RhFeLi/TiO $_2$ Com (Fig. 3). The catalytic performance of RhFeLi/TiO $_2$ NRs remains stable in a 20 h stability test (Fig. S7†). The superior reactivity and long-term

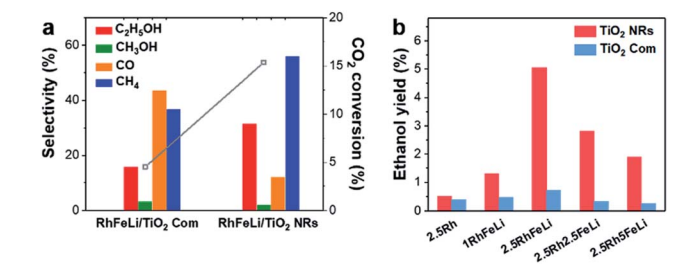


Fig. 3 (a) The CO_2 conversion (grey) and product selectivity of 2.5 wt% RhFeLi/TiO₂ NRs and 2.5 wt% RhFeLi/TiO₂ Com. (b) The ethanol yield of the Rh-based catalyst supported on TiO₂ NRs and TiO₂ Com.

stability of RhFeLi/TiO₂ NRs catalysts provide an inspiration for their potential industrial application.

Promotion effects of the hydroxyl groups

First, the hydroxyl groups were introduced by pre-reduction of RhFeLi/TiO₂ NRs and RhFeLi/TiO₂ Com catalysts in a H₂ atmosphere at 400 °C. Fourier transform infrared (FTIR) experiments were carried out to characterize the surface hydroxyl groups on RhFeLi/TiO₂ catalysts. As shown in Fig. S8,† the broad band at 3450 cm⁻¹ and the sharp peak at 1640 cm⁻¹ are assigned to the stretching and bending vibrations of associated hydroxyls, respectively.²⁹ The density of hydroxyl groups on RhFeLi/TiO₂ NRs is much higher than that on RhFeLi/TiO₂ Com (Fig. 4a), suggesting that high-density hydroxyl groups could be introduced into the catalytic system by using TiO₂ NRs. Subsequently, the catalytic properties of the hydroxyls on TiO₂

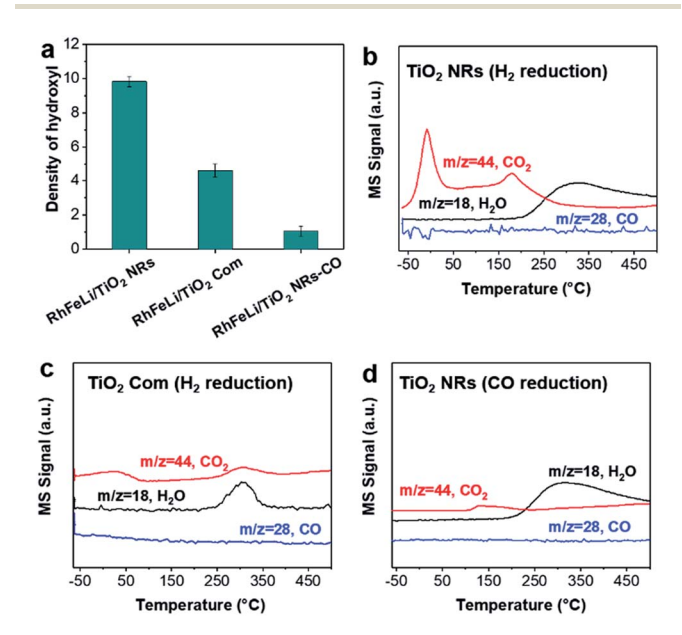


Fig. 4 (a) The peak area of hydroxyls in FTIR normalized by $S_{\rm BET}$ ($\times 10^3$) on 2.5 wt% RhFeLi/TiO $_2$ NRs, 2.5 wt% RhFeLi/TiO $_2$ Com and 2.5 wt% RhFeLi/TiO $_2$ NRs-CO. (b) CO-TPD profiles of 2.5 wt% RhFeLi/TiO $_2$ NRs. Pretreatment: H $_2$ reduction at 400 °C. (c) CO-TPD profiles of 2.5 wt% RhFeLi/TiO $_2$ Com. Pretreatment: H $_2$ reduction at 400 °C. (d) CO-TPD profiles of 2.5 wt% RhFeLi/TiO $_2$ NRs. Pretreatment: CO reduction at 350 °C.

NRs are characterized by CO temperature-programmed desorption (CO-TPD). A sharp signal peak of CO₂ (m/z=44) at \sim 0 °C is observed in CO-TPD profiles for both RhFeLi/TiO₂ NRs and pure TiO₂ NRs (Fig. 4b and S8a†). As reported previously, the CO₂ may originate from the water–gas shift process, in which the CO adsorbed on Rh sites reacts with hydroxyl groups. ^{29,30} However, a small CO₂ peak at \sim 0 °C is observed for RhFeLi/TiO₂ Com and pure TiO₂ Com due to the lack of hydroxyls (Fig. 4c and S8a†).

Chemical Science

The TOF of ethanol formed over RhFeLi/TiO2 NRs is determined to be 0.12 h⁻¹, which is much higher than that over RhFeLi/TiO₂ Com or RhFeLi/SiO₂ (0.08 h⁻¹) (Table S2†). Therefore, we suggest that the surface hydroxyl groups may play an important role in ethanol formation via CO₂ hydrogenation. To verify the role of hydroxyls in ethanol formation, the RhFeLi/ TiO2 NR catalyst was pre-treated in a CO atmosphere (RhFeLi/ TiO2 NRs-CO). The removal process of hydroxyl groups in CO was monitored by in situ diffuse reflectance infrared Fourier transform spectroscopy (DRIFTS, Fig. S9a†).31 We find that the IR peak of hydroxyl stretching vibrations (3450 cm⁻¹) disappears gradually in CO at 350 °C. The hydroxyls can be removed completely after ~12 minutes of CO-feeding (Fig. S9b†). After the pre-treatment in CO flow at 350 °C, the CO₂ peak at \sim 0 °C isn't observed in the CO-TPD profile (Fig. 4d), and RhFeLi/TiO₂ NR-CO catalysts with a hydroxyl-deficient surface are prepared (Fig. 4a and S8b†). Compared with RhFeLi/TiO2 NRs reduced with H₂, the RhFeLi/TiO₂ NRs-CO catalyst exhibits much lower CO₂ conversion (4.7%) and produces almost no ethanol (Fig. 5a). The selectivity to CO reaches ~80% among the products and the selectivity to CH₄ decreases from 53.9% to 9.6%. In the TEM images (Fig. S10†), RhFeLi/TiO2 NRs and RhFeLi/TiO2

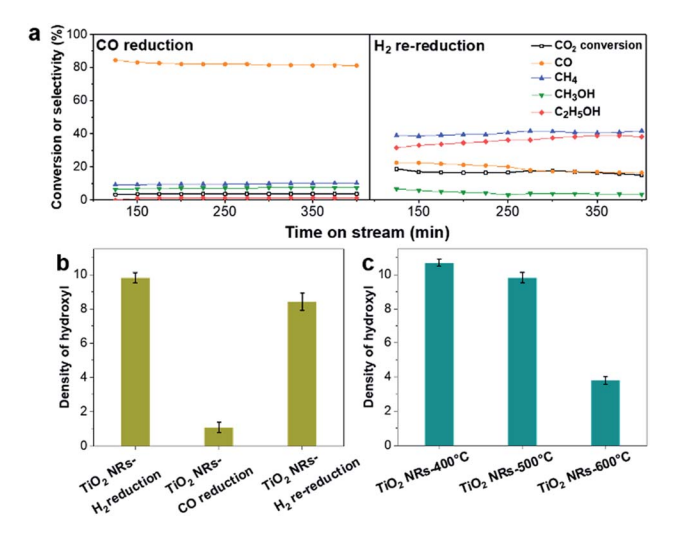


Fig. 5 (a) CO₂ conversion and product selectivity *versus* time obtained from 2.5 wt% RhFeLi/TiO₂ NRs. CO reduction was conducted at 350 °C for 0.5 h. Re-reduction in H₂ was carried out at 400 °C for 1 h. Reaction conditions: P=30 atm, T=250 °C, GHSV = 6000 h⁻¹, CO₂/H₂ = 1/3. (b) The peak area of hydroxyls in FTIR normalized by $S_{\rm BET}$ (×10³) on 2.5 wt% RhFeLi/TiO₂ NRs pretreated under different reduction atmospheres. (c) The peak area of hydroxyls in FTIR normalized by $S_{\rm BET}$ (×10³) on 2.5 wt% RhFeLi/TiO₂ NRs calcined at different temperatures.

NR-CO catalysts show similar size distribution. Besides, there is no BE shift of the XPS Rh 3d peak for RhFeLi/TiO₂ NR-CO compared with RhFeLi/TiO₂ NRs (Fig. S11, Table S4†). Therefore, the influences of the size effect and chemical state of Rh can be excluded. Instead, the decrease of the selectivity to CH₄ and ethanol should be attributed to the lack of hydroxyls. When hydroxyl groups are re-introduced by H₂ exposure (Fig. 5b and S8b†), promoted catalytic performance is achieved (35% ethanol selectivity and 18% CO₂ conversion), which is very similar to that of fresh RhFeLi/TiO₂ NRs reduced with H₂. These results further indicate that hydroxyls play an important role in tuning product distribution and promoting ethanol synthesis through CO₂ hydrogenation.

In sequential experiments, a mixture of CO2 and H2 $(CO_2: H_2 = 1:3)$ is first introduced into an *in situ* cell at 250 °C, followed by a switch to pure CO₂ flow to investigate the stability of hydroxyls and formate species. In a CO₂ + H₂ atmosphere $(CO_2: H_2 = 1:3)$ at 250 °C, the bands at 3016, 2965 and 2880 cm⁻¹ in the ν_{C-H} region appear to be stemming from gaseous CH₄ (3016 cm⁻¹) and adsorbed formate species, respectively. In the O-C-O stretching region between 1650 and 1200 cm⁻¹, the bands at 1520 and 1390 cm⁻¹ are assigned to carbonate, while the rest of the peaks may stem from adsorbed formate (1595 and 1370 cm⁻¹, Table S5†).³²⁻³⁴ The absorbance intensities of the dissociated hydroxyl stretching vibrations at 3600 cm⁻¹ and OCO asymmetric stretching vibration at 1595 cm⁻¹ in DRIFTS are used to represent the amount of hydroxyls and formate, respectively.34 As shown in Fig. 6, the changes of the hydroxyl amount and the formate amount are plotted as a function of time when switching the CO₂ + H₂ flow to pure CO2 flow at 250 °C. We find that the amounts of hydroxyls and formate species on RhFeLi/TiO2 NRs remain almost unchanged under pure CO₂ flow for 40 min (Fig. 6, S12a and c†). In contrast, the hydroxyls and formate adsorbed on RhFeLi/TiO₂ Com disappear rapidly within 20 min (Fig. 6, S12b and d†). We suggest that the abundant hydroxyl groups on RhFeLi/TiO2 NRs can stabilize the formate species, which has been proposed to be one of the intermediates of methanation via formate hydrogenation and then scission of C-O in *CH_x-O.^{18,35}

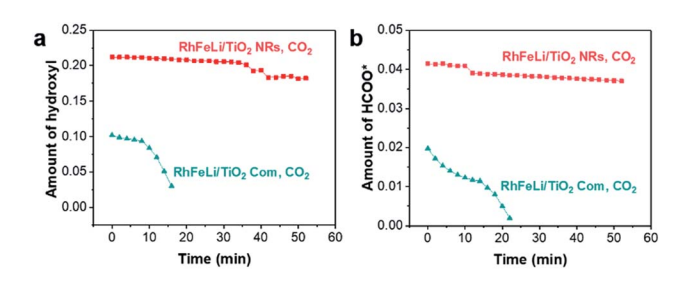


Fig. 6 (a) The absorbance intensity of hydroxyls at 3600 cm $^{-1}$ in DRIFTS of 2.5 wt% RhFeLi/TiO $_2$ NRs and 2.5 wt% RhFeLi/TiO $_2$ Com versus time after switching the CO $_2$ + H $_2$ + Ar (CO $_2$: H $_2$ = 1 : 3) flow to pure CO $_2$ flow at 250 °C. (b) The absorbance intensity of formate at 1595 cm $^{-1}$ in DRIFTS of 2.5 wt% RhFeLi/TiO $_2$ NRs and 2.5 wt% RhFeLi/TiO $_2$ Com versus time after switching the CO $_2$ + H $_2$ + Ar (CO $_2$: H $_2$ = 1 : 3) flow to pure CO $_2$ flow at 250 °C.

Edge Article

In situ DRIFTS was further carried out to investigate the catalytic role of hydroxyls in ethanol formation. In contrast to RhFeLi/TiO₂ Com, additional bands at 1470 cm⁻¹ and 1746 cm⁻¹ are observed for RhFeLi/TiO₂ NRs under a CO₂ + H₂ atmosphere ($CO_2: H_2 = 1:3$) at 250 °C (Fig. 7a). The existence of the band at 1746 cm⁻¹ has been reported for Rh/Al₂O₃ (ref. 35) and Ru/Al₂O₃ (ref. 36) catalysts, which can be attributed to adsorbed formyl (CHO*) species. It is believed that the formation of CHO* is the rate-limiting step of ethanol synthesis (Scheme S1†).12 Also, CHO* is thermodynamically more favored to be dissociated into *CH_r than into CO.^{21-23,37} As expected, significant amounts of *CH₃ species (1470 cm⁻¹) are observed on the surface of RhFeLi/TiO2 NRs (Fig. 7a). 17,18 Subsequently, CO can be inserted into these abundant adsorbed *CH₃ species on RhFeLi/TiO₂ NRs, which may be responsible for the high ethanol yield.38 Based on the above analysis, a mechanism that hydroxyls stabilize the formate and accelerate the scission of CH_x -O to produce * CH_3 species is proposed (Scheme 1).

With increasing the calcination temperature from 400 to 600 °C, the normalized peak area of associated hydroxyl vibration bands for RhFeLi/TiO₂ NRs decreases gradually, indicating that the density of hydroxyls is decreased (Fig. 5c and S8c†). In addition, the summed selectivity and TOF of CH₄ and ethanol show a downward trend with increasing the calcination temperature of TiO₂ NRs (Tables S2 and S6†). Since the RhFeLi nanoparticles show a similar size distribution (Fig. S10†) and the same electronic state of Rh and Fe as that for TiO₂ NRs calcined at various temperatures (Fig. S11, Table S4†), the

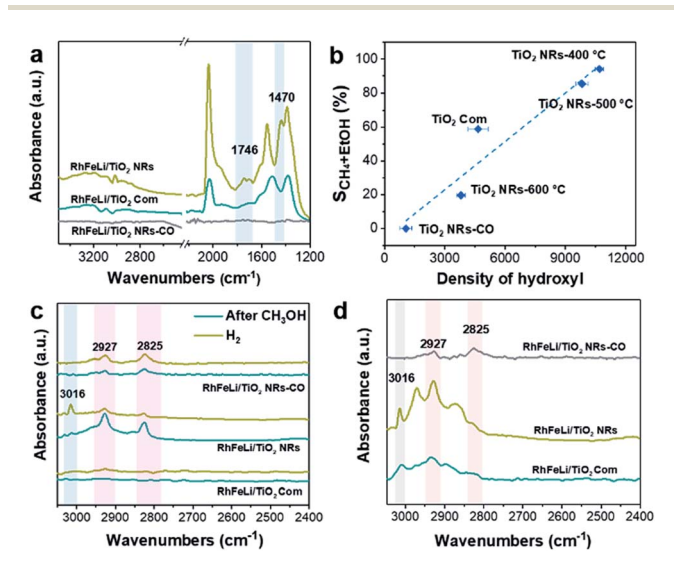
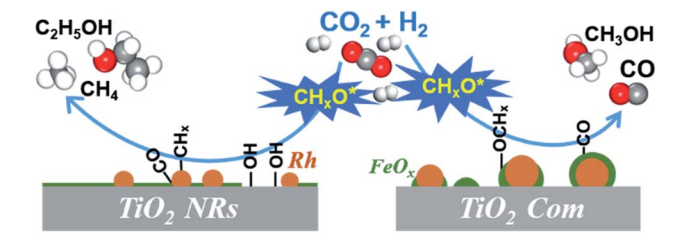


Fig. 7 (a) In situ DRIFTS of 2.5 wt% RhFeLi/TiO $_2$ NRs, 2.5 wt% RhFeLi/TiO $_2$ Com and 2.5 wt% RhFeLi/TiO $_2$ NRs-CO under a CO $_2$ + H $_2$ + Ar (CO $_2$: H $_2$ = 1 : 3) atmosphere at 250 °C. (b) The summed selectivity to CH $_4$ and ethanol as a function of the peak area of hydroxyls normalized by S_{BET} of the samples obtained from 2.5 wt% RhFeLi supported on different TiO $_2$ supports. (c) In situ DRIFTS of 2.5 wt% RhFeLi/TiO $_2$ NRs, 2.5 wt% RhFeLi/TiO $_2$ Com and 2.5 wt% RhFeLi/TiO $_2$ NRs-CO after CH $_3$ OH + Ar adsorption followed by H $_2$ adsorption at 250 °C. (d) In situ DRIFTS of 2.5 wt% RhFeLi/TiO $_2$ NRs, 2.5 wt% RhFeLi/TiO $_2$ Com and 2.5 wt% RhFeLi/TiO $_2$ NRs-CO under a CO + H $_2$ + Ar (CO : H $_2$ = 1 : 2) atmosphere at 250 °C.



Scheme 1 Schematic of CO_2 hydrogenation over the Rh-based catalyst with or without hydroxyl groups on TiO_2 . The hydroxyls play an important role in accelerating the scission of CH_x – O^* and promote the formation of ethanol.

differences in catalytic performance should be attributed to the changes of surface hydroxyls. It is noteworthy that the catalytic performance of RhFeLi/TiO₂ NRs-600 °C is comparable to that of the RhFeLi/TiO₂ NRs-CO catalyst, because there are few hydroxyls on their surfaces. Similarly, changing the support from TiO₂ NRs to TiO₂ Com can also generate a hydroxyl-deficient surface, causing the selectivity for ethanol and CH₄ to be reduced largely (Table S6†). To display the relationship between hydroxyl groups and catalytic performance directly, we take the summed amount of CH₄ and ethanol as the total amount of *CH₃, because these two products stem from *CH₃ hydrogenation and CO insertion, respectively.³⁹ As shown in Fig. 7b, the amount of *CH₃ exhibits a linear correlation with the density of hydroxyls, illustrating that hydroxyls may accelerate the scission of the C–O bond to form the *CH₃ species.

The reactions of CH₃OH and H₂ over RhFeLi/TiO₂ were conducted as well to elucidate the role of hydroxyls. The DRIFTS data were obtained after pre-treatment with CH₃OH and subsequent feeding with H₂ at 250 °C (Fig. 7c). Upon the feeding of CH₃OH, all the samples show similar CH₃O* (2825 and 2927 cm⁻¹) species.40-42 After the feeding of H2, the IR peak intensity of CH₃O* in RhFeLi/TiO₂ NRs decreases. Simultaneously, an obvious IR peak of gaseous CH₄ (3016 cm⁻¹) can be observed for RhFeLi/TiO2 NRs. The formation of CH4 could be attributed to the C-O bond scission in CH₃O* followed by *CH₃ hydrogenation. The hydroxyl groups on RhFeLi/TiO2 NRs are suggested to promote the C-O bond scission in CH₃O* to produce the *CH₃ intermediate. In contrast, the IR peak intensity of CH₃O* does not decrease, and CH4 is hardly found for RhFeLi/TiO2 Com and RhFeLi/TiO₂ NRs-CO after H₂ feeding. Therefore, it is reasonable to infer that the hydroxyls on RhFeLi/TiO2 NRs could protonate CH₃O*, i.e., promoting C-O bond scission in CH₃O* to form *CH₃. A similar phenomenon is observed under CO and H₂ at 250 °C (Fig. 7d). A sharp CH₄ peak emerges for RhFeLi/TiO₂ NRs, which is accompanied by formate (2880 and 2965 cm⁻¹) and CH₃O* (2825 and 2927 cm⁻¹). In contrast, we find only CH₃O* species adsorbed on RhFeLi/TiO2 NRs-CO. The IR peaks of gaseous CH₄ and formate are undetectable for RhFeLi/TiO₂ NRs-CO and RhFeLi/TiO2 Com, which could be attributed to the removal of hydroxyls after CO treatment.

Previous studies have proposed that ethanol can be synthesized by CO insertion into *CH₃ species to form CH₃CO*, followed by CH₃CO* hydrogenation.^{37,38} To verify this route of ethanol formation, the DRIFTS data of RhFeLi/TiO₂ NRs and

RhFeLi/TiO₂ NRs-CO were obtained after pre-treatment with CH₃OH and subsequent feeding with CO + H₂ (CO : H₂ = 1 : 1) at 250 °C (Fig. S13a†). Both gaseous and liquid products were analyzed in the reaction of CH₃OH + CO + H₂ at 250 °C (Fig. S13b†), and ethanol is the only C₂₊ product. Hence, the appearance of the methylene peak (2858 cm⁻¹) for RhFeLi/TiO₂ NRs indicates the C–C coupling and formation of ethanol.⁴³ However, methylene, *i.e.*, ethanol is not formed over RhFeLi/TiO₂ NRs-CO. According to these data, the high ethanol selectivity of RhFeLi/TiO₂ NRs might be attributed to the high-density hydroxyls, which enhance the C–O bond scission to produce *CH_x intermediates for the CO insertion.

Surface functionalization with hydroxyls is frequently applied to promote the catalytic performance of catalysts.44-47 The role of surface hydroxyls has often been considered to modulate the local concentration of hydrophilic reactants, such as alcohols, around the active sites. For example, the hydrophobic treatment of Pd/MOF improves its catalytic activity for styrene hydrogenation by increasing the interaction between hydrophobic reactants and Pd sites.48 In formaldehyde oxidation reaction, the abundant hydroxyl groups nearby the Pt active sites can also facilitate formate oxidation through the formation of the Pt/Ni(OH)_x interface.⁴⁹ In CO₂ hydrogenation reaction, hydroxyl groups on hydrophilic SiC quantum dots can promote methanol formation via a H-transfer mechanism, in which the diffusion of H from hydroxyl groups to CO2 assists the formation of the intermediate HCOO*.50 Here, our work clearly demonstrates the catalytic role of hydroxyl groups in ethanol synthesis via CO2 hydrogenation. We show that the surface hydroxyl species on RhFeLi/TiO2 NRs can protonate methanol and reduce the energy barrier for C-O bond scission, facilitating the generation of *CH3 species. Accordingly, CO obtained from RWGS can be inserted into abundant *CH₃ species to form CH₃CO*, followed by CH₃CO* hydrogenation to ethanol.

Conclusions

Chemical Science

In conclusion, we have demonstrated the crucial role of surface hydroxyls on the RhFeLi/TiO₂ NR catalyst in the synthesis of ethanol from CO₂ hydrogenation. Based on *in situ* spectroscopic characterization, we propose two advantages of the TiO₂ NR support for CO₂ hydrogenation to ethanol: (i) Rhbased nanoparticles are highly dispersed on TiO₂ NRs due to the strong interaction between the catalyst and TiO₂ NR support, thus displaying high activity; (ii) abundant hydroxyls on TiO₂ NRs can protonate methanol, which is easily dissociated into *CH_x, thus favoring the formation of ethanol upon CO insertion. This work not only provides the detailed understanding of the catalytic role of hydroxyls in heterogeneous catalysis but also opens an avenue for developing efficient catalysts for CO₂ conversion.

Experimental section

Chemicals

TiO₂ NRs were prepared by hydrothermal treatment of a mixture of titanium tetrachloride, nitric acid and water.^{51,52} Briefly,

titanium tetrachloride (TiCl₄, Shanghai Chemical Reagent Co., 98%) was dissolved in ultrapure water in an ice-water bath to obtain a 3 M TiCl₄ solution. Subsequently, 35 mL aliquot of concentrated nitric acid (HNO₃, 15 M) was refluxed in a silicone oil bath and heated to 200 °C gradually, and then 20 mL of the 3 M titanium tetrachloride solution was rapidly injected into nitric acid under vigorous stirring. After aging for 20 h, the autoclave was cooled to room temperature. The obtained precipitates were centrifuged and washed several times with deionized water and ethanol. The filtered solid was dried at 100 °C in a vacuum overnight and calcined at 300, 400, 500 and 600 °C for 4 h, respectively (denoted as TiO₂ NRs-*x* °C). Unless otherwise specified, TiO₂ NRs are denoted as TiO₂ NRs-500 °C. The commercial TiO₂ (TiO₂ Com) was purchased from Alfa Aesar Chemical Co. Ltd for comparison.

RhCl $_3 \cdot n H_2 O$ (Huaweiruike Chemical Co., 99%), LiNO $_3$ (Alfa Aesar Chemical Co. Ltd., 98%) and Fe(NO $_3$) $_3 \cdot 9 H_2 O$ (Alfa Aesar Chemical Co. Ltd., 98%) were used as precursors and a series of reducible metal oxides (MO) were used as the support. MO (1 g) were impregnated with distilled water (1 mL) containing the precursor by using ultrasonication for 1 h. Generally, the molar ratio of Rh and promoters was 1 : 1 unless specified. Subsequently, the sample was dried at room temperature overnight and then at 80 °C for 10 h. Finally, the sample was calcined in air at 300–500 °C for 4 h and reduced in pure H_2 at 400 °C for 2 h. The element loading was based on the weight ratio of Rh and Fe with respect to MO supports.

Hydrogenation of CO₂

All the catalytic reactions were carried out in a fixed-bed microreactor. In a typical experiment, 300 mg of each catalyst with a 20-40 mesh size distribution was mixed with 2.0 g of quartz particles (SiC: granulation of 0.075-0.4 mm) to avoid hot spots and pressure drop across the bed and packed in a stainless steel (ϕ 8 × 400 mm) tubular reactor. Prior to each experiment, the catalyst was activated by reduction in a H₂ atmosphere (99.99%) with a flow rate of 30 mL min $^{-1}$ and a temperature of 400 $^{\circ}$ C for 1 h. The RhFeLi/TiO2 NRs-CO sample was obtained from RhFeLi/ TiO2 NRs-500 °C reduced under CO flow at 350 °C for 0.5 h. After the reduction of the catalyst, the reactor was cooled down to reaction temperature. Then the reactant gases (CO2 and H2 with a molar ratio of 1:3, 30 bar) were introduced into the reactor. The gas hourly space velocity (GHSV) was set at 6000 h^{-1} . The product gas was analyzed with an online gas chromatograph (GC, Agilent 7890B) equipped with two detectors. One is a flame ionization detector (FID) with a HP-FFAP column using H2 as a carrier gas to analyze the organic species such as alcohols, oxygenates and hydrocarbons. The other one is a thermal conductivity detector (TCD) with columns of MS-5A and Hayesep Q using He as a carrier gas to monitor the non-condensable gas species including H2, CO2, N2, CO and CH4. All the flows between the reactor and the GC were heated and maintained beyond 150 °C, to avoid the liquefaction of the alcohol products.

Conflicts of interest

There are no conflicts to declare.

Acknowledgements

This work was financially supported by the National Key R&D Program of China (2016YFB0600901), the National Natural Science Foundation of China (21525626, 21603159, 21676181), and the Program of Introducing Talents of Discipline to Universities (B06006).

References

Edge Article

- 1 M. Aresta, A. Dibenedetto and A. Angelini, *Chem. Rev.*, 2014, **114**, 1709–1742.
- 2 W. Wang, S. Wang, X. Ma and J. Gong, Chem. Soc. Rev., 2011, 40, 3703–3727.
- 3 H. Yang, C. Zhang, P. Gao, H. Wang, X. Li, L. Zhong, W. Wei and Y. Sun, *Catal. Sci. Technol.*, 2017, 7, 4580–4598.
- 4 A. Swapnesh, V. C. Srivastava and I. D. Mall, *Chem. Eng. Technol.*, 2014, 37, 1765–1777.
- 5 Z. He, Q. Qian, J. Ma, Q. Meng, H. J. Zhou, H. J. Song, Z. Liu and B. Han, *Angew. Chem., Int. Ed.*, 2016, **128**, 747–751.
- 6 D. L. S. Nieskens, D. Ferrari, Y. Liu and R. Kolonko, *Catal. Commun.*, 2011, 14, 111–113.
- 7 T. Inui, T. Yamamoto, M. Inoue, H. Hara, T. Takeguchi and J. B. Kim, *Appl. Catal.*, *A*, 1999, **186**, 395–406.
- 8 M. Takagawa, A. Okamoto, H. Fujimura, Y. Izawa and H. Arakawa, *Stud. Surf. Sci. Catal.*, 1998, 114, 525–528.
- 9 S. Li, H. Guo, C. Luo, H. Zhang, L. Xiong, X. Chen and L. Ma, *Catal. Lett.*, 2013, **143**, 345–355.
- 10 H. Kusama, K. Okabe, K. Sayama and H. Arakawa, *Energy*, 1997, 22, 343–348.
- 11 H. Kusama, K. Okabe, K. Sayama and H. Arakawa, *Catal. Today*, 1996, **28**, 261–266.
- 12 Y. Choi and P. Liu, J. Am. Chem. Soc., 2009, 131, 13054-13061.
- 13 N. Yang, A. J. Medford, X. Liu, F. Studt, T. Bligaard, S. F. Bent and J. K. Norskov, *J. Am. Chem. Soc.*, 2016, 138, 3705–3714.
- 14 Y. Wang, H. Luo, D. Liang and X. Bao, *J. Catal.*, 2000, **196**, 46–55.
- 15 R. G. Zhang, M. Peng and B. J. Wang, *Catal. Sci. Technol.*, 2017, 7, 1073–1085.
- 16 J. C. Matsubu, V. N. Yang and P. Christopher, *J. Am. Chem. Soc.*, 2015, **137**, 3076–3084.
- 17 S. Kattel, W. Yu, X. Yang, B. Yan, Y. Huang, W. Wan, P. Liu and J. G. Chen, *Angew. Chem., Int. Ed.*, 2016, 55, 7968–7973.
- 18 S. Kattel, P. Liu and J. G. Chen, J. Am. Chem. Soc., 2017, 139, 9739–9754.
- 19 D. Wang, Q. Bi, G. Yin, W. Zhao, F. Huang, X. Xie and M. Jiang, Chem. Commun., 2016, 52, 14226–14229.
- 20 S. Bai, Q. Shao, P. Wang, Q. Dai, X. Wang and X. Huang, *J. Am. Chem. Soc.*, 2017, **139**, 6827–6830.
- 21 R. Burch and M. J. Hayes, J. Catal., 1997, 165, 249-261.
- 22 J. Xu, X. Su, H. Duan, B. Hou, Q. Lin, X. Liu, X. Pan, G. Pei, H. Geng, Y. Huang and T. Zhang, J. Catal., 2016, 333, 227– 237
- 23 R. Zhang, B. Wang, H. Liu and L. Ling, J. Phys. Chem. C, 2011, 115, 19811–19818.

- 24 J. Lee, D. C. Sorescu and X. Y. Deng, *J. Am. Chem. Soc.*, 2011, 133, 10066–10069.
- 25 L. Liu, C. Zhao and Y. J. Li, J. Phys. Chem. C, 2012, 116, 7904–7912.
- 26 J. Z. Y. Tan, Y. Fernández, D. Liu, M. Maroto-Valer, J. Bian and X. Zhang, *Chem. Phys. Lett.*, 2012, **531**, 149–154.
- 27 J. C. Matsubu, S. Zhang, L. DeRita, N. S. Marinkovic, J. G. Chen, G. W. Graham, X. Pan and P. Christopher, *Nat. Chem.*, 2017, 9, 120–127.
- 28 T. Huizinga, H. F. J. van 'T Blik, J. C. Vis and R. Prins, Surf. Sci., 1983, 135, 580-596.
- 29 Z. Xu, J. Yu and M. Jaroniec, *Appl. Catal.*, *B*, 2015, **163**, 306–312.
- 30 T. Yang, Y. Huo, Y. Liu, Z. Rui and H. Ji, *Appl. Catal., B*, 2017, **200**, 543–551.
- 31 X. Zou, Z. Rui, S. Song and H. Ji, J. Catal., 2016, 338, 192-201.
- 32 J. Graciani, K. Mudiyanselage, F. Xu, A. E. Baber, J. Evans, S. D. Senanayake, D. J. Stacchiola, P. Liu, J. Hrbek, J. Fernandez Sanz and J. A. Rodriguez, *Science*, 2014, 345, 546–550.
- 33 X. Wang, Y. Hong, H. Shi and J. Szanyi, *J. Catal.*, 2016, 343, 185–195.
- 34 X. Wang, H. Shi and J. Szanyi, Nat. Commun., 2017, 8, 513.
- 35 D. Heyl, U. Rodemerck and U. Bentrup, *ACS Catal.*, 2016, **6**, 6275–6284.
- 36 P. S. Eckle, H.-G. Anfang and R. J. Behm, *J. Phys. Chem. C*, 2011, **115**, 1361–1367.
- 37 R. Zhang, G. Wang, B. Wang and L. Ling, *J. Phys. Chem. C*, 2014, **118**, 5243–5254.
- 38 Y. H. Zhao, K. Sun, X. Ma, J. Liu, D. Sun, H. Y. Su and W. X. Li, *Angew. Chem., Int. Ed. Engl.*, 2011, **50**, 5335–5338.
- 39 G. Prieto, P. Concepción, A. Martínez and E. Mendoza, *J. Catal.*, 2011, 280, 274–488.
- 40 J. Wang, G. Li, Z. Li, C. Tang, Z. Feng, H. An, H. Liu, T. Liu and C. Li, *Sci. Adv.*, 2017, 3, e1701290.
- 41 I. A. Fisher and A. T. Bell, J. Catal., 1997, 172, 222-237.
- 42 A. Goguet, F. C. Meunier, D. Tibiletti, J. P. Breen and R. Burch, *J. Phys. Chem. B*, 2004, **108**, 20240–20246.
- 43 M. A. Natal-Santiago and J. A. Dumesic, *J. Catal.*, 1998, 175, 252–268.
- 44 Y. Dai, S. Liu and N. Zheng, *J. Am. Chem. Soc.*, 2014, **136**, 5583–5586.
- 45 Q. Sun, B. Aguila, G. Verma, X. Liu, Z. Dai, F. Deng, X. Meng, F.-S. Xiao and S. Ma, *Chem*, 2016, **1**, 628–639.
- 46 F. Liu, W. Kong, C. Qi, L. Zhu and F.-S. Xiao, *ACS Catal.*, 2012, **2**, 565–572.
- 47 J.-D. Lin, Q.-Y. Bi, L. Tao, T. Jiang, Y.-M. Liu, H.-Y. He, Y. Cao and Y.-D. Wang, *ACS Catal.*, 2017, 7, 1720–1727.
- 48 G. Huang, Q. Yang, Q. Xu, S. Yu and H. Jiang, *Angew. Chem.*, *Int. Ed.*, 2016, 55, 7379–7383.
- 49 T. Yang, Y. Huo, Y. Liu, Z. Rui and H. Ji, *Appl. Catal., B*, 2017, **200**, 543–551.
- 50 Y. H. Peng, L. B. Wang, Q. Q. Luo, Y. Cao, Y. Z. Dai, Z. L. Li, H. L. Li, X. S. Zheng, W. S. Yan, J. L. Yang and J. Zeng, *Chem*, 2018, 4, 613–625.
- 51 Q. Huang and L. Gao, Chem. Lett., 2003, 32, 638-639.
- 52 Q. Zhang and L. Gao, Langmuir, 2003, 19, 967–971.